energies

MDPI

Article

CFD and PIV Investigation of a Liquid Flow Maldistribution across a Tube Bundle in the Shell-and-Tube Heat Exchanger with Segmental Baffles

Grzegorz Ligus [1,*], Marek Wasilewski [2], Szymon Kołodziej [1] and Daniel Zając [3]

[1] Faculty of Mechanical Engineering, Opole University of Technology, 45-758 Opole, Poland; s.kolodziej@po.edu.pl
[2] Faculty of Production Engineering and Logistics, Opole University of Technology, 45-758 Opole, Poland; m.wasilewski@po.opole.pl
[3] Engineering and R&D Department, Kelvion Sp. z o. o., 45-641 Opole, Poland; daniel.zajac@kelvion.com
* Correspondence: g.ligus@po.edu.pl

Received: 31 July 2020; Accepted: 28 September 2020; Published: 2 October 2020

Abstract: The paper presents the results of research on liquid flow maldistribution in the shell side of a shell-and-tube heat exchanger (STHE). This phenomenon constitutes the reason for the formation of the velocity reduction area and adversely affects heat transfer and pressure drop. In order to provide details of the liquid distribution in STHE, two visualization methods were utilized. First, computational fluid dynamics (CFD) code coupled with the k-ε model and the laser-based particle image velocimetry (PIV) technique was applied. The tests were carried out for a bundle comprising 37 tubes in an in-line layout with a pitch $d_z/t = 1.5$, placed in a shell with $D_{in} = 0.1$ m. The STHE liquid feed rates corresponded to Reynolds numbers Re_{in} equal to 16,662, 24,993, and 33,324. The analysis demonstrated that the flow maldistribution in the investigated geometry originates the result of three main streams in the cross-section of the shell side: central stream, oblique stream, and bypass stream. For central and oblique streams, the largest velocity reduction areas were formed in the wake of the tubes. On the basis of the flow visualization, it was also shown that the in-line layout of the tube bundle helps to boost the wake region between successive tubes in a row. Additionally, unfavorable vortex phenomena between the last row of tubes and the lower part of the exchanger shell were identified in the investigations. The conducted studies confirmed the feasibility of both methods in the identification and assessment of fluid flow irregularities in STHE. The maximum error of the CFD method in comparison to the experimental methods did not exceed 7% in terms of the pressure drops and 11% in the range of the maximum velocities.

Keywords: CFD; PIV; shell-and-tube; shell side; tube bundle; heat exchanger; baffle; maldistribution

1. Introduction

Shell-and-tube heat exchangers (STHEs) find widespread applications in industry. They are utilized not only in areas whose purpose is only heat exchange but also in devices that are applied to perform other processes in technology. Consequently, the performance of many processes is dependent on the operating parameters of heat exchangers. The improvement of the operating parameters of heat exchangers is associated mainly with the need to perform geometric modifications sometimes leading to the comprehensive redesign of heat exchangers and thus the development of new types of devices. Another direction of modifications can be associated with material use that ensures better heat transfer parameters coupled with adequate strength parameters of heat exchangers. Extensive research is also

carried out in the areas concerned with selecting optimal parameters of fluid flow in the heat exchanger. One of the first significant modifications to the STHE was associated with the use of segmental baffles in the shell side. The use of baffles leads to the fluid flow in such a way that its turbulence is increased, which directly contributes to the improvement of the performance of the heat exchangers. Although new heat exchanger designs have emerged in recent years, STHEs are still a standard solution in many cases and in some cases forms the only viable solution. Today, the development research of industrial flow equipment is most often carried out in two stages. Initially, analysis using computational fluid dynamics (CFD) is performed, whose main purpose involves the selection the most suitable alternative of the investigated parameters among many possibilities. Then, experimental verification of selected parameters is performed. In this area, in particular, methods based on optical techniques are recognized in all fields of engineering and contribute to a significant increase in the reliability of the results gained on the basis of CFD codes. One of the most popular techniques currently utilized for this purpose is particle image velocimetry (PIV). It is one of the laser-based methods that allows the representation and analysis of the velocity fields in an investigated region. As a consequence, PIV offers a complementary tool to the application of CFD. Numerical and experimental investigations of classical STHEs with baffles are often undertaken in a variety of papers (see the following sections). However, little research has dealt with identifying flow structures and examining flow maldistribution across the tube bundle. The aim of this paper is to demonstrate the role taken by the adequate selection of flow parameters in the generation of variations of the local flow velocity in the device, which in turn led to flow maldistribution. In addition, the results should serve to provide assistance to an extensive group of researchers who carry out CFD tests in flow systems containing tube bundles in a variety of devices.

1.1. Insights from Literature in the Field of CFD Application in Heat Exchangers

Following the rapid development of computer techniques, research applying CFD methods is becoming increasingly common. Due to a number of advantages (e.g., low research costs, easy design modifications in the investigated devices, access to the common results), this method can provide the ready solution to the ever increasing economic and technical demand for devices applied in chemical and process engineering. The CFD method has been successfully applied on many occasions in research concerned with the description of the flow and heat transfer phenomena and the optimization of heat exchangers. When we perform an analysis of research on using the CFD method in heat exchangers, we can make particular reference to the study reported by Bhutta et al. [1], which forms an overview of the studies carried out by application of this method. The authors state that the CFD method was applied in the studies involving fluid flow maldistribution, pressure drop and thermal analysis, fouling, and in the design and optimization phases. A variety of interesting results can be found in the area of plate-fin heat exchangers, where flow maldistribution forms one of the major factors affecting the decrease of the effective heat exchange [2–4].

Kim et al. [5] performed an assessment of the types of flow patterns in STHE. For this purpose, three types of headers were investigated: A, B, and C. The conclusion is that the design with the longest fin offers the best performance. Ozden et al. [6] carried out a study by application of the same type of the heat exchanger. The conclusion section contains a statement that few recirculation regions are formed at the rear of the baffles when the number of baffles is small.

A large proportion of research works takes on the subjects concerned with the aspects of pressure drop reduction. Wang and Dong [7] conducted the research on various types of supporting structures applied for STHEs. The authors concluded that their geometry forms an important aspect in terms of the performance of the devices. As a result of the comparison of six types of supporting structures, it was demonstrated that rod elements are the most reliable and suitable supporting structure with a minimum pressure drop.

The study by Wang et al. [8] contains a statement that the pressure drop of a combined multiple shell-pass shell-and-tube heat exchanger tends to be lower than shell-and-tube heat exchanger with segmental baffles, for the same heat transfer conditions by almost 13%. Mohammadi et al. [9]

demonstrated that the heat exchanger comprising a horizontal baffle has a 20% higher heat transfer coefficient combined with 250% greater pressure drop than the one with vertical baffles. Other examples of works concerned with STHEs and focusing on heat exchange aspects include articles Ozden and Tari [6] and Raj and Velraj [10].

A noteworthy research is reported in Sun et al. [11]. The authors investigated the effects of the application of inclined trefoil-hole baffles on the performance of STHEs. For this purpose, a comparison of this design with a similar model of the heat exchanger equipped with segmented baffles was performed. The comparison of numerical calculations demonstrated that the heat transfer coefficient in the exchanger with inclined trefoil-hole baffles is lower by 23.89% than in the exchanger with standard segmented baffles. However, a significant decrease in pressure drop was observed (pressure drop decrease was equal to 44.19%), which resulted in the higher specific value of the heat transfer coefficient related to the pressure drop by 36.38% than in the traditional heat exchanger design. The literature also contains studies on fouling in various types of heat exchangers (e.g., Jun and Puri [12], De Bonis and Ruocco [13]).

A detailed analysis of the studies available in the field of CFD application and concerned with heat exchangers indicates that several models can be applied to successfully represent turbulent flow. The obtained experimental results have repeatedly confirmed the compliance of CFD applications with the results of other research techniques in the validation processes. The standard k-ε model forms the most commonly model applied in the literature. The use of this model ensures high compliance of CFD test results with experimental tests (the range of the error in the analyzed works was from 2% to 10%) with the minimum possible load of computational units [1].

1.2. Insights from the Literature in the Field of PIV Application in Heat Exchangers

The common applications of the PIV method in the studies concerned with heat exchangers often involve studies concerned with the effect of the geometry of individual structural elements on either hydrodynamics or aerodynamics of the fluid flow. Such issues were raised e.g., by Iwaki et al. [14]. Using the PIV method, the study investigated the variations in the hydrodynamic characteristics of liquid flow across the tube bundle depending on the layout of the tubes in the bundle. The experiments were performed for in-line and staggered bundles with a pitch to diameter ratio of 1.5. The research demonstrated that parameters such as velocity distribution, flow structures, wake, and turbulent structures in the tube bundles should be taken into account when heat exchangers are designed, as formation of these structures is considerably dependent on the geometrical conditions in which fluid flow occurs. During the measurements, it was noted that turbulence for the staggered system behind the second row of pipes increases to a greater extent than for the in-line system. It was also confirmed that the flow in the staggered system was more homogeneous, since such geometry results in the mixing of flow streams and stabilization of the flow structure over a shorter distance. The extension of the above research to be applied with regard to the conditions of two-phase gas-liquid flow can be found in study: Vertical, bubbly, cross-flow characteristics over tube bundles [15]. In a study conducted in a system with a similar geometry, it was found that despite the fact that the difference in turbulence intensity between two configurations decreased in comparison to two-phase and single-phase conditions, the degree of turbulence in a staggered system still remains higher than in an in-line system. An important conclusion contained in this publication also includes the confirmation of the possibility of the application of computer image analysis in the measurement of velocities of both the liquid and gas phases and in the determination of the void fractions.

More complex shell-side geometry was previously investigated (e.g., Zhang et al. [16]), where the investigation involved the distribution of oil flow in a disc-type transformer winding. Despite the difficult imaging, it was noted that total volume of liquid derived from the PIV measurements is constantly slightly higher compared to the results gained by measurements using a flowmeter. The authors also pointed out that the end-wall effects in such geometry are usually neglected. We can

note that such effects should be considered important in the experimental research concerned with various types of shell-side designs in heat exchangers.

The first attempt of visualizing PIV flow in an industrial heat exchanger was reported in paper Planar PIV experiments inside a transparent shell-and-tube exchanger [17]. This investigation involved the classic STHE with an internal diameter of 0.301 m and a bundle of 54 tubes with a diameter of 0.2 m. The authors carried out their research in their subsequent works (Turbulent flow in a no-tube-in-window shell-and-tube heat exchanger [18], Two-Phase Flow Regimes in Exchangers and Piping: Part 1. [19]), where a description was provided of the case of the shell side with four segmental baffles, for which the characteristic velocity contours were determined in different span-wise locations. It was indicated in the study that individual streamlines are superimposed as well as stagnation points are identified. In the research, it was clearly demonstrated that in the case of testing of flows in as complex geometries as in the case of shell side, it is very important to combine experimental research and CFD.

The literature also includes research on fluid distribution systems in heat exchangers. Tests of this type were carried out in the shell side as well as in the tube side. Wang et al. [20] investigated the effects of the introduction of two types of porous baffles installed with the purpose of regulating fluid distribution in the inlet part to the tube side and in the splitter bar to the tubes. It was found that the use of porous baffles can lead to a significant improvement of the fluid distribution. The comparison of the straight and arc baffle demonstrated that the latter offers better performance of the rectification process. In contrast, the introduction of a splitter bar into the tubes effectively reduces vortex formation in the tube side.

The issues associated with improvement of fluid distribution in heat exchanger tubes were also reported in article PIV measurement of flow structures in a circular heat exchange tube with central slant rod inserts [21]. The authors determined the liquid flow velocity fields in a circular heat exchange tube with central slant rod inserts using the stereoPIV method and additionally, on the basis of CFD simulations, the characteristics of heat transfer were determined. This study also demonstrated that the number of generated vortices is relative to the geometry of the central slant rod and the vortex intensity increases with the increase of the Reynolds number. The uncertainty of the velocity field measurement was also estimated, and it was demonstrated that the maximum relative errors for the velocities in the x, y and z directions are equal to approximately 3%, 6%, and 1.5%, respectively. The work also included a comparison of the results obtained by CFD simulations and experiment results using the stereoPIV technique, and it was found that the deviations of vorticity and z-velocity distribution are found within the range of 8% and 5%, respectively. Therefore, the study contains a conclusion that the overall efficiency of heat transfer in tubes equipped with central slant rod inserts is reliable.

The analysis of fluid flow in the shell side was also investigated by Lee at al. [22] and Delgado at al. [23]. The two works report the results of flow visualization using the PIV method in a helical coil steam generator. In the research, the authors observed several dark regions resulting from the difficulties of applying the PIV method for the analysis in the shell side. In order to improve the measurement methodology in the work of Delgado at al. [24], the optical system was coupled with a Scheimpflug module and a computer image correction was applied, and consequently, the image was converted from trapezoidal to rectangular. The authors noted, however, that the use of the Scheimpflug module resulted in a maldistribution of the light and led to shadow formation in the tube bundle. Hence, it was therefore necessary to use a Gaussian distribution for the color scale and the image brightness was increased by 20% for the purposes of obtaining better identification of seeding particles on this side of the image, where illumination was unsatisfactory. Besides, Im at al. [25] discussed obstacles faced during imaging process in the shell side. In the case of large field of view, a greater part of the area that could be potentially applied for flow analysis of the shell side was obstructed by horizontal heating rods. Consequently, the velocity vectors in these areas were found to be incorrect. This problem did not occur in the case of local measurements using small fields of view.

The effect of segmented baffles on the STHE performance was analyzed by Chang et al. in [26]. Tests were performed by application of a heat exchanger with two baffles located along a tube bundle. Velocity profiles between the baffles for co-current and countercurrent flow were determined for this purpose. CFD simulations were also performed, the results of which were identical to the reported PIV experiment. The paper also discussed the effect resulting from the presence of an intense liquid stream in the bottom part of the shell side. This phenomenon was linked to clearance between the baffle and the shell of heat exchanger. During the research, a zone of large circulation behind the baffle was also identified. There were also differences in the liquid distribution depending on the technique applied to feed fluid into the heat exchanger.

A testing procedure carried out along the tube bundle for the case of a heat exchanger comprising helicoidal baffles was reported by Wen et al. [27]. In this case, researchers conducted an experiment with the purpose of comparing standard plain helical baffles with an improved fold helical baffle design in which a triangular gap forming between adjacent baffles was embedded. The upgraded baffle made it possible to obtain better heat transfer characteristics coupled with virtually unchanged pressure drops. The performance of such a heat exchanger increased in the same flow conditions in the range from 2% to 8%, and the results correlated very well with the analysis of velocity field changes obtained on the basis of PIV tests.

In the summary of the literature in the field of PIV research concerned with heat exchangers, we can note the widespread use of this technique. The analyzed cases apply a wide range of geometries and flow parameters and in the conditions combined with adequately selected measurement methodology, the results derived from PIV measurements are well simulated by means of computer techniques as well as other experimental measurement techniques.

1.3. The Research Gap and the Adopted Target of the Study

As we can see from Sections 1.1 and 1.2, studies of the flow maldistribution in STHEs have so far been carried out mainly in model rectangular geometries, along a tube bundle, or due to the perspective phenomenon in a limited region captured by a camera. While reviewing the state of the art, papers could not be found that address the subjects related to simultaneous CFD and PIV studies of fluid flow maldistribution in STHE on an industrial scale, with segmented baffles across a tube bundle and carried out by means of imaging of the complete cross-section the shell side. There were also no works concerned with identifying and analyzing the role of fluctuating vortex phenomena occurring in the bottom part of the shell side. Currently, designers and operators of STHE obtain information about the flow in these devices primarily from industry standards. Therefore, extending the state of knowledge with data obtained with the use of modern non-invasive measurement methods forms an important task from many points of view. Validation of the numerical model and assessment of the flow in the actual geometry of the cross-section of a tube bundle, taking into account the synergy of a variety of geometric and flow factors form a novelty in this research. Therefore, the purpose of the research was the use of CFD and PIV methods to demonstrate the role taken on by flow and geometrical parameters in the generation of variations of the local flow velocities in the device, which in turn lead to flow maldistribution and evolution of flow structures in the shell side. In addition, the results should serve to provide assistance to an extensive group of researchers who carry out CFD and PIV tests in flow systems containing tube bundles in a variety of devices.

2. Materials and Methods

2.1. Numerical Model and Computational Scheme

In numerical research, finite volume method (FVM) was utilized for the analysis of flow fields and flow parameters on the basis of Ansys Fluent CFD code. The pressure-based solution method segregated solver was applied for this purpose. The pressure-velocity coupling was performed with the semi-implicit method for pressure linked equations (SIMPLE) algorithm [28]. This algorithm

was successfully utilized in research concerned with heat exchangers in a number of works [29–35]. Second-order upwind interpolation was used to determine representative samples of component values on the control volume surface and standard wall function. Variable values of under-relaxation factors were determined. They were equal to 0.6, 0.5, 0.8, and 0.8 for the pressure, momentum, turbulent kinetic energy, and turbulent energy dissipation, respectively. The following convergence criteria were adopted: 1×10^{-7} for the continuity equations, and 1×10^{-5} for others. Boundary conditions for the inlet: "velocity inlet" (turbulence intensity: 5%, hydraulic diameter: 0.1); for the outlet: "pressure outlet." A no slip boundary condition was used along the surface of the heat exchanger. Figure 1 presents the computational domain in an isometric view.

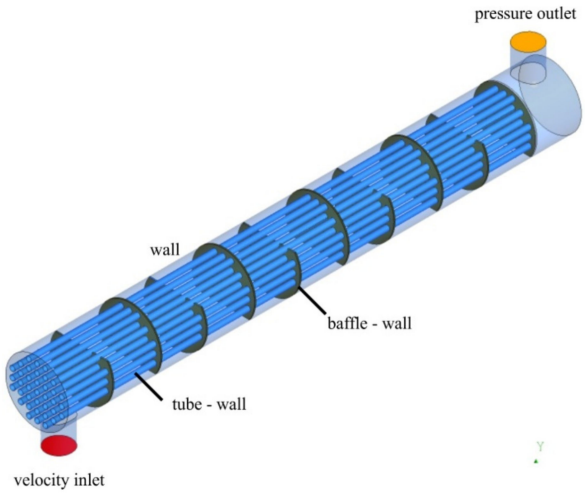

Figure 1. Isometric view of the computational domain.

The standard k-ε model was used as a closing model in simulations of turbulent flow incorporating Reynolds-averaged Navier–Stokes equations (RANS). It has been widely used for CFD research on heat exchangers [29–34,36]. The governing equations in the computational domain are presented in the following forms [37]:
continuity part:

$$\frac{\partial u_j}{\partial x_j} = 0 \tag{1}$$

momentum part:

$$\rho \frac{\partial \left(u_i u_j\right)}{\partial x_j} = -\frac{\partial p_i}{\partial x_i} + \frac{\partial}{\partial x_j}\left[\mu\left(\frac{\partial u_i}{\partial x_j} + \frac{\partial u_j}{\partial x_i}\right)\right] \tag{2}$$

energy part:

$$\rho \frac{\partial \left(u_j T\right)}{\partial x_j} = \frac{\partial}{\partial x_j}\left(\frac{\lambda}{C_p}\frac{\partial T}{\partial x_j}\right) \tag{3}$$

where u is the averaged velocity of the fluid [m/s]; p is pressure; ρ is the density of the fluid; T is temperature; μ is the kinematic viscosity of the fluid [m^2/s]; C_p is the specific heat capacity [J/kgK]; and λ is the thermal conductivity [W/mK].

The regular k–e model is adopted to simulate turbulent flow in present paper, which is presented as:
turbulent kinetic energy part:

$$\rho \frac{\partial (k u_i)}{\partial x_i} = \frac{\partial}{\partial x_j}\left[\left(\mu + \frac{\mu_T}{\sigma_k}\right)\frac{\partial k}{\partial x_j}\right] + G_k - \rho\varepsilon \tag{4}$$

turbulent energy dissipation part:

$$\rho\frac{\partial(\varepsilon u_i)}{\partial x_i} = \frac{\partial}{\partial x_j}\left[\left(\mu + \frac{\mu_T}{\sigma_\varepsilon}\right)\frac{\partial \varepsilon}{\partial x_j}\right] + \frac{C_{1\varepsilon}\varepsilon}{k}G_k - C_{2\varepsilon}\rho\frac{\varepsilon^2}{k} \quad (5)$$

where k is turbulent kinetic energy [m^2/s^2], ε is turbulent dissipation rate [m^2/s^3], G_k is producing term of turbulent kinetic energy generated by mean velocity gradient, $C_{1\varepsilon}$ and $C_{2\varepsilon}$ are constants, σ_ε and σ_k are Prandtl numbers corresponding to turbulent kinetic energy and turbulent dissipation rate, and μ_T [Pas] is expressed as

$$\mu_T = \rho C_\mu \frac{k^2}{\varepsilon} \quad (6)$$

where C_μ = 0.09 [-], $C_{1\varepsilon}$ = 1.44 [-], $C_{2\varepsilon}$ = 1.92 [-], σ_k = 1.0 [-], σ_ε = 1.3 [-], and G_k [-] is defined as

$$G_k = -\rho\overline{u_i' u_j'}\frac{\partial u_j}{\partial x_i} \quad (7)$$

2.2. Application of Particle Image Velocimetry Technique

The PIV technique forms one of the most common experimental methods that is applicable for verification of CFD models. It forms an optical method in which specific conditions of an experiment have to be fulfilled. It is necessary to ensure the transparency of the surface of the investigated device and illumination of the selected plane of the device with a coherent light, and thus the formation of a laser sheet plane. The illuminated phenomena are registered with a camera synchronized with the light source. In order to visualize the flow of the fluid, it is necessary to add suitably selected inert seeding particles to it in order to match the flow and physicochemical parameters of the fluid. The PIV technique uses the relationship between the displacement (in direction x and y defined as Δx and Δy respectively) of seeding particles recorded in the images and the known time between subsequent images often referred to as time between laser pulses Δt. Taking into account the above, the velocities u and v defined as Δx/Δt and Δy/Δt are calculated. On this basis, with the use of statistical methods, the velocity vector V which is expressed as $\sqrt{u^2 + v^2}$ can be determined (Figure 2).

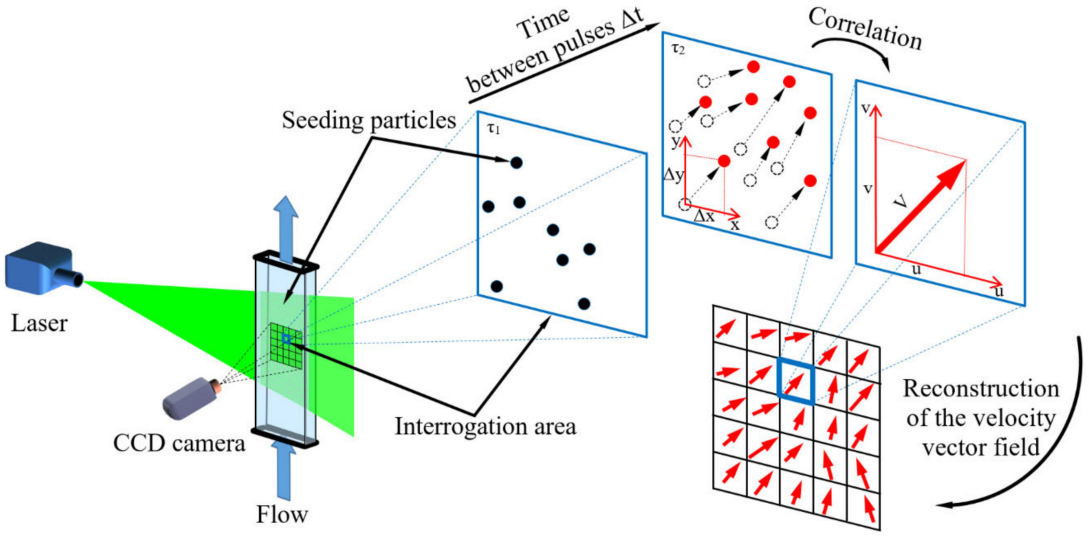

Figure 2. Idea of measurements applying the particle image velocimetry (PIV) technique.

In the research, the planar PIV method was used to visualize the fluid velocity field across a tube bundle. The model of the tested heat exchanger was made of Poly(methyl 2-methylpropenoate) (PMMA). Inside the exchanger, in the shell with an internal diameter D = 0.244 m, a tube bundle was installed, consisting of 37 tubes with an external diameter D_z = 0.02 m, mounted on 10 segmented

baffles with a cut of 25%. Since the goal of the research involved the analysis of the phenomena in the shell side, the exchanger model did not include either head chambers or tubesheets; therefore, the fluid flow did not occur in the tube side (as the tubes were sealed on both sides). Water formed the fluid applied in the tests, and it was circulated in a sealed system. The liquid was extracted by a Grundfos CR5-7 pump (Grundfos, Bjerringbro, Denmark) from a tank with the capacity of 0.2 m^3 and routed through a pipeline to the heat exchanger, and then returned to the tank. The pump was controlled by a signal from the ENKO EM-005C electromagnetic flowmeter (ENKO, Gliwice, Poland). The applied PIV method required that seeding particles were introduced into the flow. Fluorescent seeding particles PMMA-RHB-10 stained with rhodamine B were applied for this purpose. A stirrer was installed in the tank to maintain constant homogenization of the water. The type and number of seeding particles were determined on the basis of Adrian and Westerweel [38] and own research. The hydrodynamic characteristics of the heat exchanger model were evaluated for three liquid flow rates equal to 5 m^3/h (Re_{in} = 16,662), 7.5 m^3/h (Re_{in} = 24,993), and 10 m^3/h (Re_{in} = 33,324), respectively. These values corresponded to the inlet velocity v_{in} of 0.177 m/s, 0.266 m/s, and 0.354 m/s respectively. A Dantec Dynamics FlowSense EO-4M CCD camera (Dantec Dynamics, Skovlunde, Denmark) was installed in perpendicular plane to the cross-sectional plane of the shell side. The image was recorded at a resolution of 2048 × 2048 pixels in the double frame mode with a frequency of 10 Hz. The time between pulses was equal to 750, 500 and 300 µs for the flow rates of 5 m^3/h, 7.5 m^3/h, and 10 m^3/h, respectively. Two hundred double frame images were taken for each series of measurements. The measurement area was illuminated by a Dantec Dynamics DualPower TR Nd: YAG laser (Dantec Dynamics, Skovlunde, Denmark) via a laser sheet targeting mirror in such a way as to provide illumination of the imaging plane in a distance of 0.010 m from the last segmental baffle and in distance L_2 = 0.0135 m from the end of tube bundle. The justification for the selecting this location of the measurement plane is presented in Section 2.3. The optical system of the camera is equipped with an Omega Optical 550LP filter (Omega Optical Inc., Brattleboro, VT, USA), which cuts off more than 98% of the transmission of the light wave for wavelengths shorter from 5.5×10^{-7} m. As a result, no laser light with a wavelength of 5.32×10^{-7} m reaches the camera matrix, but only excited light emitted by fluorescent seeding particles, as it is characterized by the range of wavelength from 6.1×10^{-7} m to 6.5×10^{-7} m, i.e., above the cut-off threshold. The PIV calculations were performed using Dantec Dynamics Dynamic Studio software, ver. 2015a (Dantec Dynamics, Skovlunde, Denmark). The obtained test results are based on the analysis of the components of velocity u and v and the inlet velocity v_{in}. For the purposes of determining measure scale factor, a target located in the same plane as the generated laser sheet was used. During image calibration, no optical distortions were identified characteristic of imaging through curved surfaces or in the StereoPIV technique, where the cameras are inclined in relation to the measurement plane [38,39]. The use of images without optical correction, recorded in analogous optical paths, is common in the planar PIV technique [40–43]. Due to the assumed distance from the laser sheet and the size of the recorded image, the parallax error was not prevented. As a result, the field of view around the outer tubes in the tube bundle was excluded from analysis at a maximum distance of 1.07 mm (40 pixels) from the tube edge. Following the discussion in the work of Adrian and Westerweel [38], the uncertainty of estimating the displacement of seeding particles and the uncertainty of determining the velocity vectors have the greatest influence on an accuracy of the PIV measurement. Based on these two parameters, the maximum uncertainty of velocity determination in this experiment was set at 12%, which is illustrated by the corresponding error bars in Section 3.2.

The methodology of PIV calculations and analysis used during the research is presented in Figure 3. Figure 4 presents the scheme of the measuring station. Detailed dimensions of the model can be found in Figure 5 and Table 1.

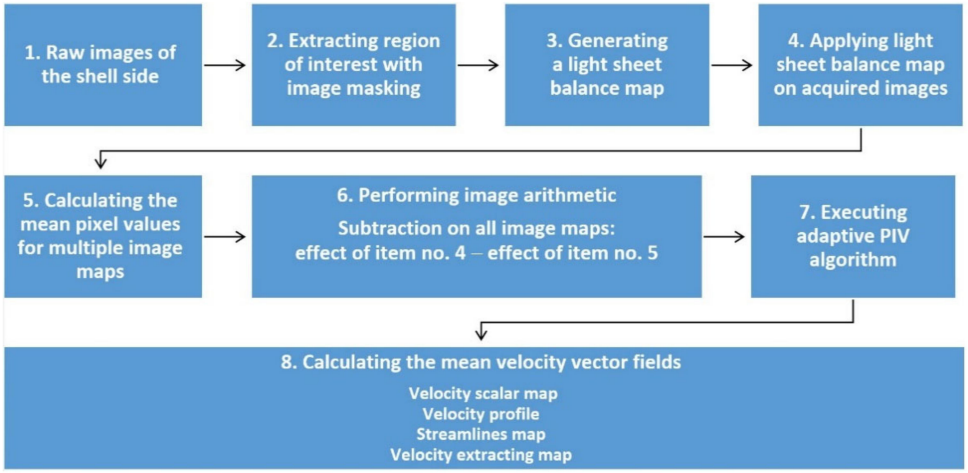

Figure 3. Applied PIV methodology.

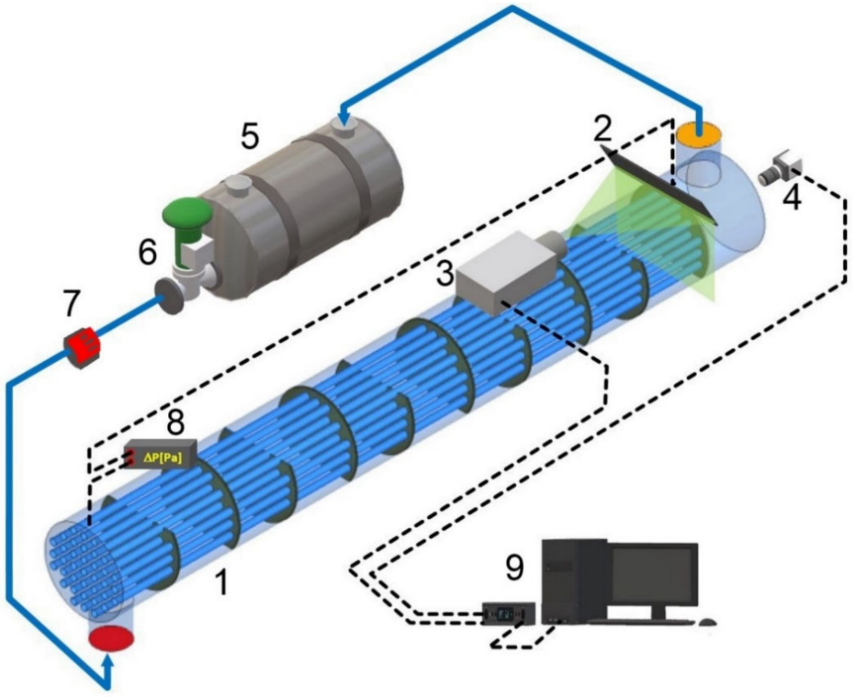

Figure 4. Experimental stand: shell-and-tube heat exchanger model (**1**), mirror (**2**), laser (**3**), CCD camera (**4**), tank (**5**), pump (**6**), flowmeter (**7**), differential pressure transmitter (**8**), and control and data acquisition station (**9**).

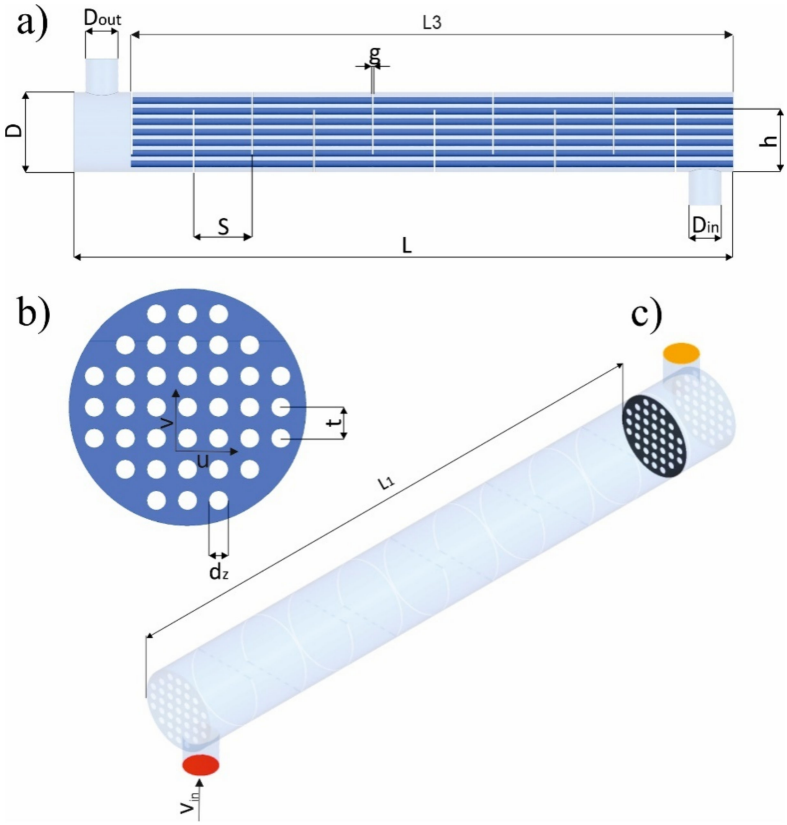

Figure 5. Geometry of the tested shell-and-tube heat exchanger (STHE) model. (**a**) Longitudinal section of the sell side; (**b**) cross-section of the shell side with the directions of velocities u and v; (**c**) location of the measuring area with direction of the velocity v_{in}.

Table 1. Detailed dimensions of the model.

Dimension	Value, m
D	0.244
D_{out}	0.1
D_{in}	0.1
S	0.178
g	0.0035
L	2
h	0.183
t	0.030
d_z	0.020
L1	1.7665
L2	0.0135
L3	1.8213

2.3. Assumptions and Conditions Applied in the Research

From the literature review we can note that the problem of perspective poses a challenge in the research applying tube bundles. The variable position of each tube in the bundle depending on its distance leads to the interferences in the visibility of the measurements (by obscuring the region of interest). This problem was already reported in previous works [22,25]. One of the solutions used in such conditions is to adjust an index of refraction of the fluid to the material from which the tubes are made. The results of the application of such approaches are presented in references [14,22]. In the current research, another solution was proposed, which involved the removal of the fraction of the tube bundle that obstructs the region of interest. CFD tests were carried out, and the results demonstrate

that the removal of the tube section behind the final baffle only slightly affects the flow characteristics (Figure 6). The maximum differences of the dimensionless parameters defining the velocities differ by a maximum of 3.5%, which does not exceed the absolute differences between the results gained from simulations and ones gained on the basis of the experimental procedure. The pressure drops also vary within a small range that does not exceed 3%. Therefore, it was concluded that the geometric modifications performed in this research could provide a solution to the problem of perspective in visualizations across tube bundles.

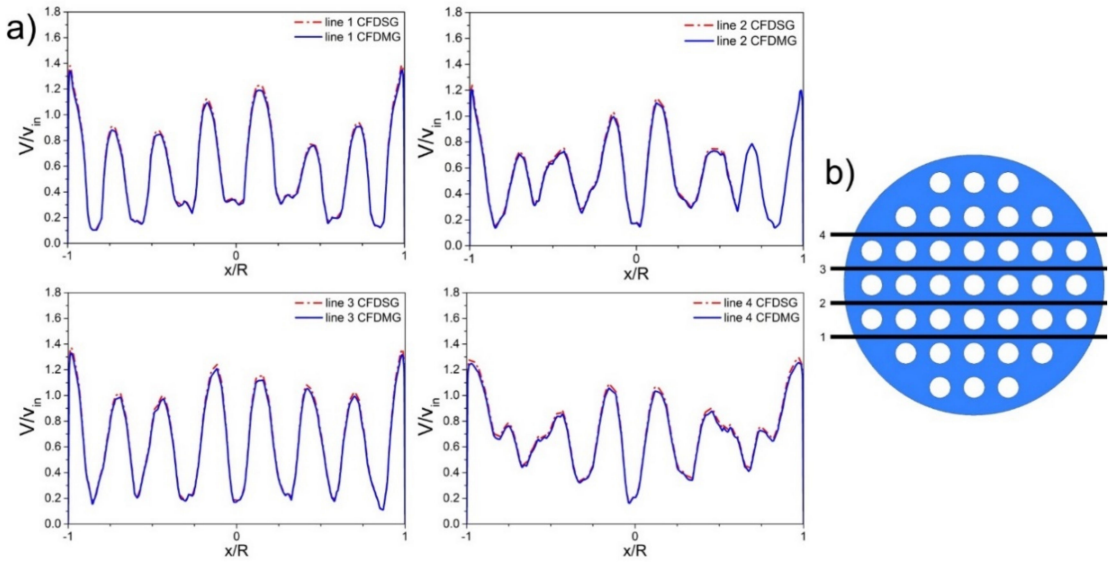

Figure 6. Comparison of velocity profiles for standard and modified tube bundle geometry. (**a**) Velocity profiles for Q = 5 m^3/h; (**b**) location of the lines 1–4.

3. Results and Discussion

3.1. Analysis of Sensitivity of Computational Mesh and Validation of Research Method

3.1.1. Analysis of Sensitivity of Computational Mesh

Before the discretization of the computational region was performed, the results were analyzed in terms of the optimization of the computational mesh. It was found that in the case of 3D heat exchanger models, tetrahedral type cells are most often employed in research. Therefore, inside the apparatus, a hybrid mesh with tetrahedral cells was utilized. Additionally, in order to maintain the correct density and proper values of the bridging functions in the shell side, a densified, five-layer mesh with hexahedral cells was used. In the next step, sensitivity analysis of the computational mesh density was performed. Four meshes with various densities were generated for this purpose (mesh 1: 8,435,989 elements; mesh 2: 10,266,557 elements; mesh 3: 12,112,572 elements; mesh 4: 12,972,099 elements). The layout of mesh cross-sections utilized in the research is presented in Figure 7. The reference for the sensitivity analysis applied the values of the recorded pressure drop in the heat exchanger (in relation to the results of experimental tests for the flow rate of 10 m^3/h) and the maximum velocities in the plane selected for the analysis. It was found that the mesh no. 3 offered considerable level of the consistency of the results combined with the lowest possible load of the computing resources (therefore, mesh 3 was included in further research). Additionally, by analyzing the obtained values of these parameters for the first three meshes, we can conclude that their values increase with the increase in the mesh density. In turn, for the fourth mesh with the greatest density, the results did not demonstrate a further increase in the values of the analyzed parameters. To illustrate this phenomenon, the obtained velocity distributions for individual meshes in the analyzed plane are presented in Figure 8. Additionally, Figure 9 shows the velocity distribution along an example of line 2 along the

analyzed plane. A complete list of the analyzed numerical meshes coupled with the results is presented in Table 2.

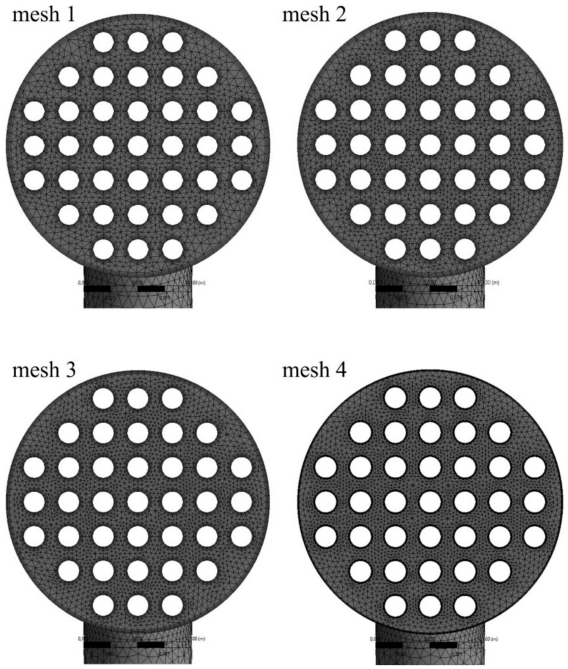

Figure 7. Layout of mesh cross-sections.

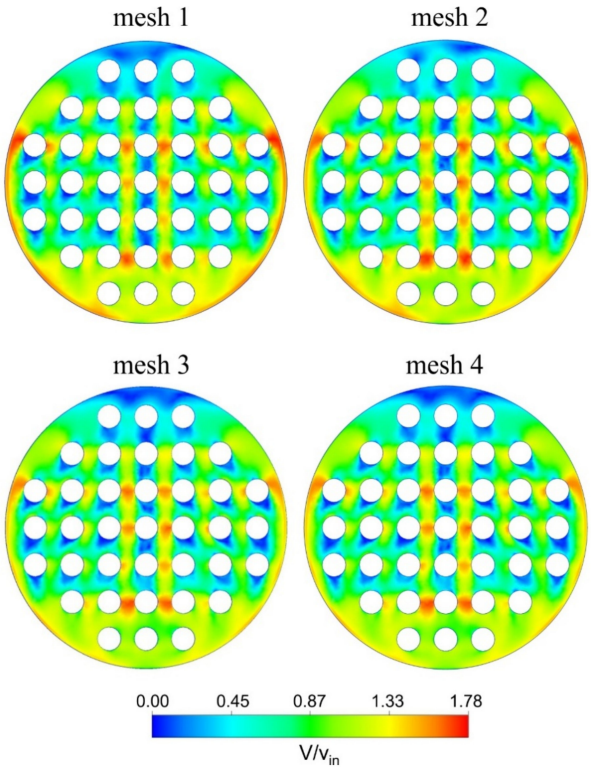

Figure 8. Velocity contours for analyzed geometric meshes.

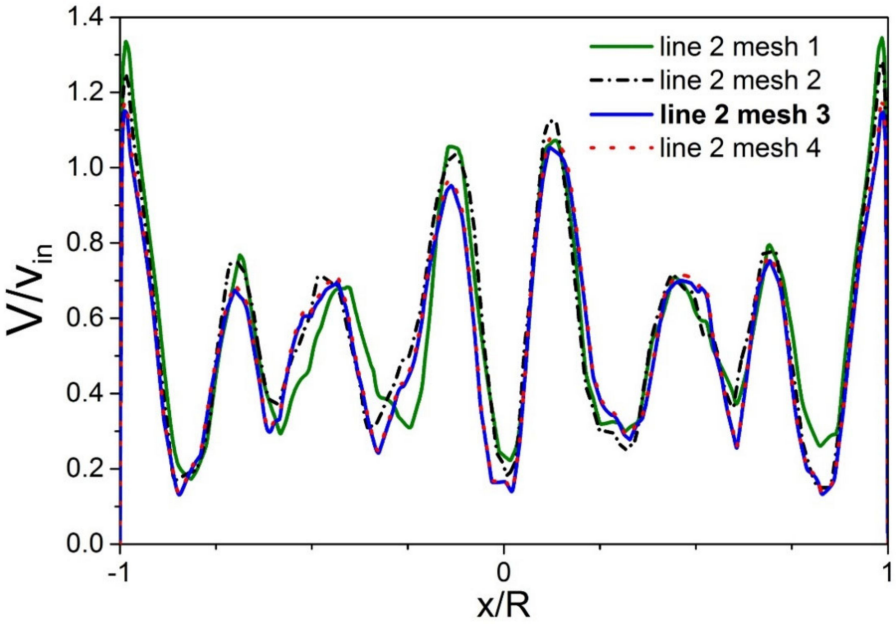

Figure 9. Velocity distributions for analyzed geometric meshes in line 2.

Table 2. Characteristics of computational fluid dynamics (CFD) meshes.

Parameter	Mesh 1	Mesh 2	Mesh 3	Mesh 4	Experimental Results and PIV
Total number of elements	8,435,989	10,266,557	12,112,572	12,972,099	—
Mean skewness	0.25	0.24	0.23	0.23	—
Maximum velocity [m/s]	0.68	0.67	0.65	0.65	0.58
Results compatibility [%]	85	87	89	89	—
Pressure drop ΔP [Pa]	2960	2930	2900	2904	2698
Results compatibility [%]	91	92	93	93	—

3.1.2. Validation of Research Methods

When several methods are used in research, it is necessary to validate the obtained results to ensure their credibility. For the purposes of this study, the results of investigations using CFD were validated by application of the results of experimental tests (in terms of pressure drop) and the PIV method (in terms of the velocity values obtained in the selected plane). The comparison was performed by application of three analyzed values of the volumetric flow rate (5 m^3/h, 7.5 m^3/h, and 10 m^3/h). Table 3 presents the results of the comparative analysis. In the case of the pressure drop value, the calculation error was equal to, respectively, for Q = 5 m^3/h—2%, for Q = 7.5 m^3/h—2%, and for Q = 10 m^3/h—7%. On the basis of the comparison of the second of the analyzed parameters (maximum velocity), the authors noted that the values of calculation errors were equal to: 10%, 10%, and 11%, respectively. In the case of the third of the considered parameters (mean velocity), the following calculation errors were noted: 6%, 8%, 9% for Q = 5 m^3/h, 7.5 m^3/h, and 10 m^3/h, respectively.

Table 3. Validation of the results.

Parameter	Value		
Volumetric Flow rate [m^3/h]	5	7.5	10
Pressure drop (CFD) [Pa]	758	1693	2900
Pressure drop (exp. results) [Pa]	746	1656	2698
Results compatibility [%]	98	98	93
Maximum velocity CFD [m/s]	0.31	0.5	0.65
Maximum velocity PIV [m/s]	0.28	0.45	0.58
Results compatibility [%]	90	90	89
Mean velocity CFD [m/s]	0.17	0.26	0.35
Mean velocity PIV [m/s]	0.16	0.24	0.32
Results compatibility [%]	94	92	91

The obtained compatibility of both the pressure drop and the flow velocity is high and can form the basis for the statement that the adopted procedures, numerical models, and parameterization of the calculation conditions applied in the research process were adequate.

3.2. *Analysis of a Liquid Flow Maldistribution across the Tube Bundle*

One of the methods applicable for evaluating the maldistribution of the liquid flow through a tube bundle involves the analysis of velocity fields. This paper presents the results of the reconstruction of scalar velocity fields derived by both the PIV and CFD methods. On this basis, regions located in the cross-section of the shell side are identified, in which flow maldistribution occurs as a result of rapid variations in the hydrodynamic parameters of the liquid over time. The intensification of flow maldistribution in the shell side often leads to the development of adverse wake regions behind the tube. In these regions, the efficiency of the heat transfer process decreases. Flow visualization analysis can be applied for the purposes of locating zones that negatively affect the performance of heat exchangers, as well as those with a fully developed flow around the tubes. In Figures 10–12, in the central row of tubes in the bundle, we can observe typical zones with clearly reduced local velocity. They are located in the wake of each tube and have an orientation that is parallel to the direction of liquid flow. When an analysis is performed of the successive rows of tubes, and moving from the center of the shell, one can observe oblique deviations of the velocity reduction zones. This phenomenon is clearly symmetrical.

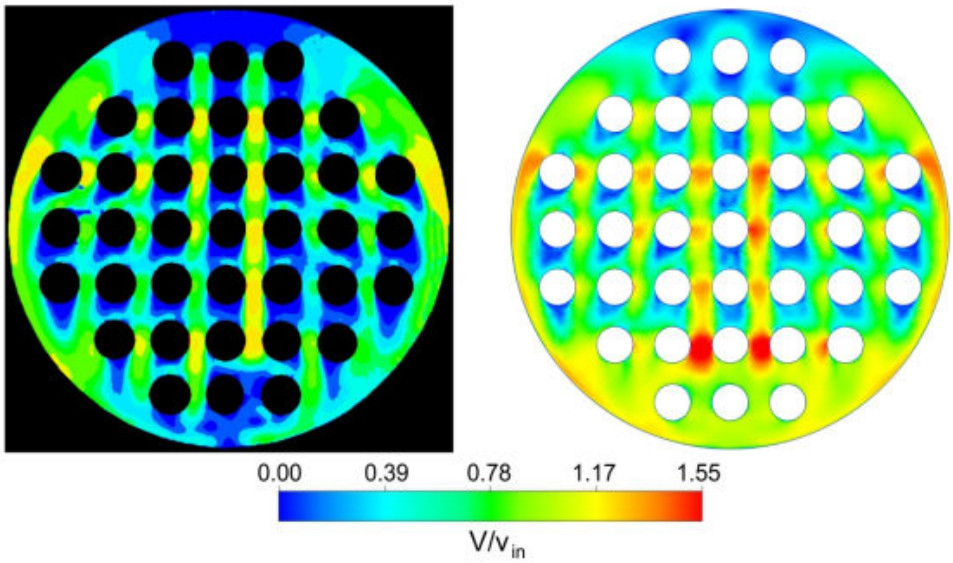

Figure 10. Comparison of scalar velocity fields V/v_{in} for Q = 5m^3/h (CFD on the right, PIV on the left).

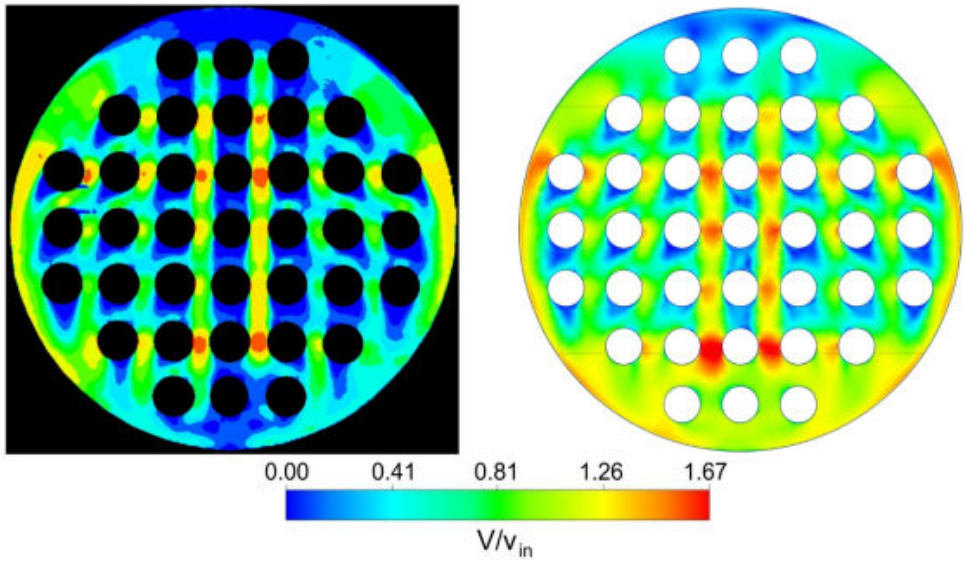

Figure 11. Comparison of scalar velocity fields V/v_{in} for Q = 7.5m^3/h (CFD on the right, PIV on the left).

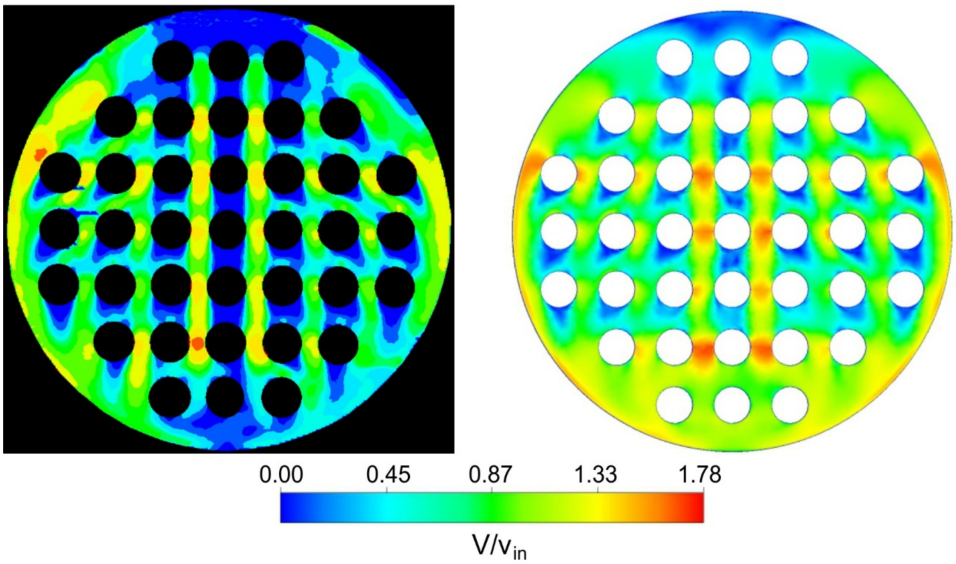

Figure 12. Comparison of scalar velocity fields V/v_{in} for Q = 10 m^3/h (CFD on the right, PIV on the left).

In addition, we can also note that the increase in the inflow rate of the liquid from Q = 5 m^3/h to Q = 7.5 m^3/h did not significantly affect the flow homogeneity or the distribution of the wake regions behind the tubes. However, a further increase in the flow rate to Q = 10 m^3/h resulted in the increase in velocity in these regions and their further reduction. The determination of the velocity profiles in the lines 1–4 marked in Figure 13 made it possible to quantify this observation (Figures 14–16). Thus, the variations in the velocity V/v_{in} in individual rows of tubes were compared for the flow rates of Q = 7.5 m^3/h and Q = 10 m^3/h. Consequently, it was observed that the increase in the flow rate Q from 7.5 m^3/h to 10 m^3/h leads to a moderate increase in the mean velocity V/v_{in} by 20%, 10.42%, 6.25%, and 4.83% for the first, second, third, and fourth velocity profiles. Besides, on the basis of the comparison of the results obtained from PIV tests and calculations using CFD, we should note that the general flow diagrams overlap in most of the investigated cases. On the basis of the analysis of the velocity profiles in vertical lines (lines 5–8 in Figure 13), it was noted that the fluctuations of the liquid flow velocity may provide assistance in defining the start-up zone. In each of the analyzed cases, the fully developed flow specific for the middle part of the cross-section of the shell side, was developed only from the point when the first clear maximum of the velocity V/v_{in} was reached. In this region,

there is a satisfactory compliance of the results gained by CFD and PIV methods. However, in the regions occupied by the first rows of tubes (both the horizontal and vertical velocity profiles) there were significant differences between the experimental and numerical results. It should be assumed that this is the effect of dynamic changes in this zone, where both the k-e model and the adopted PIV system parameters offer less accurate results. This is justified by the simplification applied in the calculation method, which does not take into account all the details of the multi-parameter flow evolution in this area, as well as the limitations of the experimental method, one drawback of which is associated with the decrease in the reliability in the regions characterized by considerable dynamic characteristics of velocity fluctuations. In regions characterized by smooth flow, the degree of conformity is satisfactory and does not exceed 10% of the maximum velocities. However, on the basis of the visual analysis of the flow, we can state that in the case of flow studies in the shell side, the CFD method provides results with smaller degree of detail in comparison to the application of PIV.

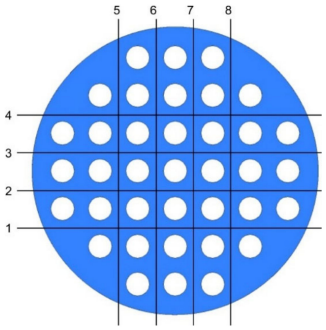

Figure 13. Location of lines applied for data extraction for purposes of determining velocity profiles.

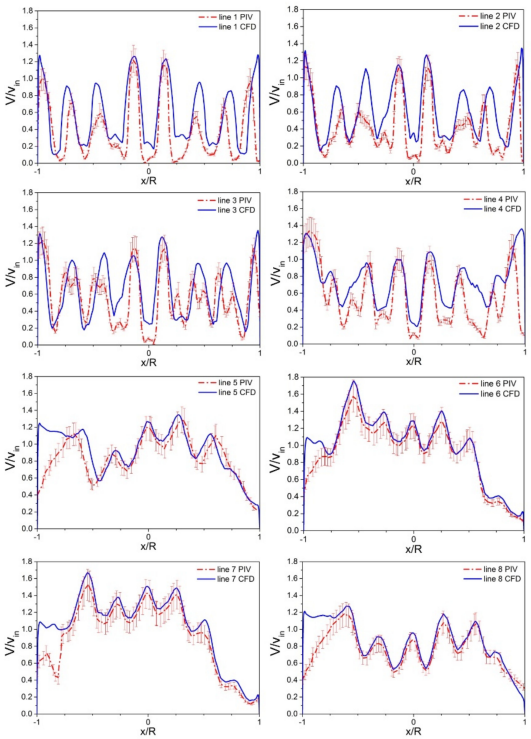

Figure 14. Comparison of velocity profiles derived by CFD method and gained from PIV for Q = 5 m^3/h.

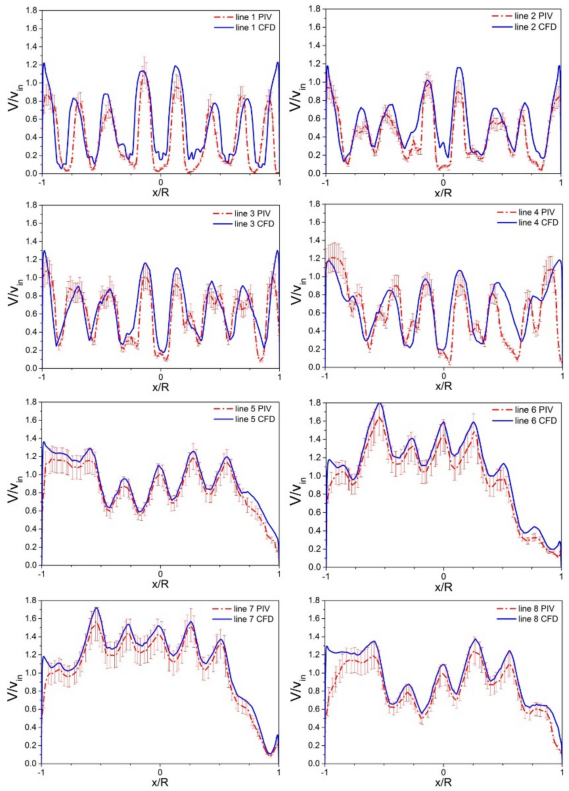

Figure 15. Comparison of velocity profiles derived by CFD method and gained from PIV for Q = 7.5 m^3/h.

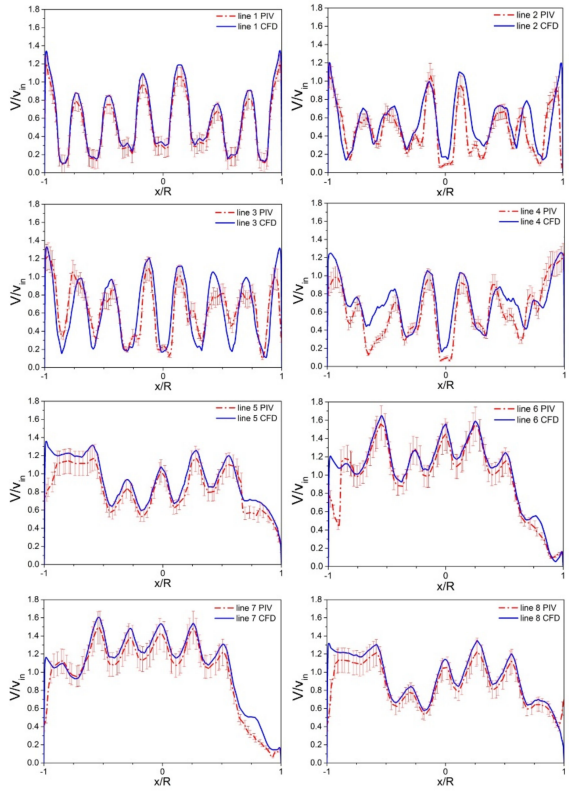

Figure 16. Comparison of velocity profiles derived by CFD method and gained from PIV for Q = 10 m^3/h.

The subsequent stage of the research into the maldistribution of the flow through shell side in STHE involved the analysis of the details on the direction of liquid flow. For this purpose, the vector

velocity field and streamlines were applied. The enlarged region of the vector velocity field marked in Figure 17 indicates a satisfactory compliance of the results gained by the CFD and PIV methods. In both cases the converging regions and the diverging regions have been recognized, as well as quantitative velocity distribution along the successive rows of tubes was identified. The calculated results also demonstrate that the velocity reduction areas always form in the wake of the tubes, on the opposite side of the tubes in relation to the direction of the liquid inflow. Liquid streams flowing obliquely between the tubes are characterized by velocity that is clearly above the mean for the entire cross-section of the shell. It is one of the main factors responsible for the formation of swirl centers in the wake of the tubes. In these regions, the velocity also drops to values close to the minimum. However, due to the fact that an in-line tube bundle layout was applied in the research, the distance between oblique tubes in the consecutive rows is greater from the distance between the tubes in the same rows. As a result, velocity reduction areas do not extend to the subsequent tube rows (see also Figures 10–12). They are also characterized by a lower velocity gradient. Under such flow conditions ahead of the next tube, the velocity of the liquid increases, which can be considered a positive phenomenon.

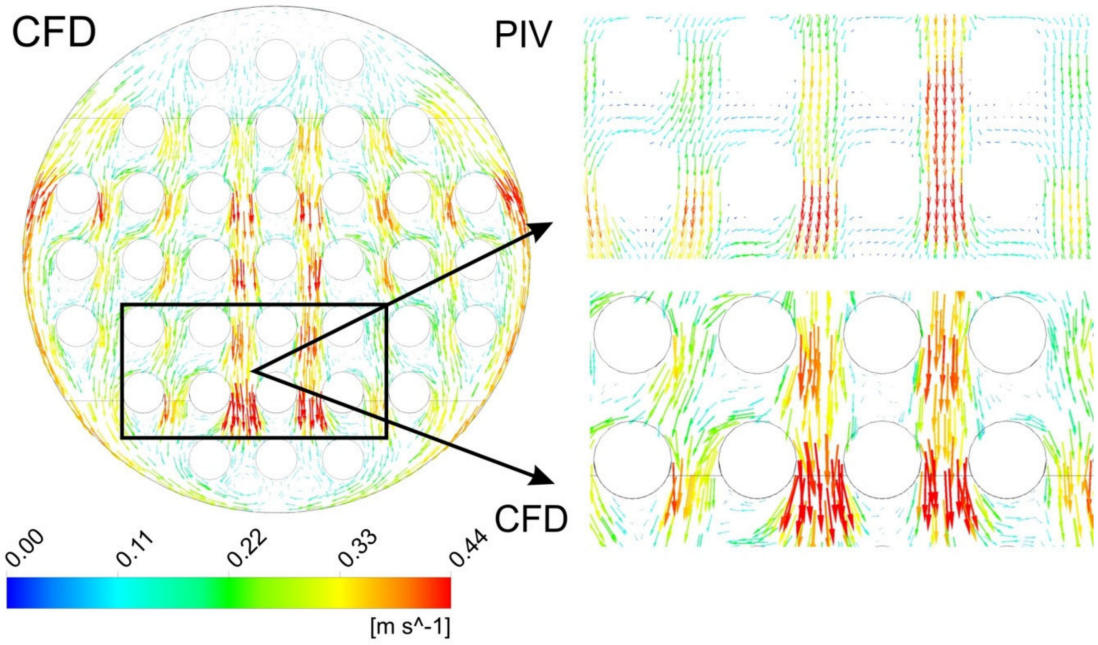

Figure 17. Sample comparison of vector velocity fields PIV and CFD for flow rate Q = 7.5 m^3/h.

Throughout the streamline analysis, both in the case of CFD and PIV method (Figure 18), the central streams, oblique streams and bypass streams were identified, and, very importantly, large vortex cells in the lower part of the shell side. The area occupied by the generated vortex comprised the lower surfaces of the last row of tubes and in particular the central tube. This vortex pattern is influenced by the central liquid stream and the two bypass streams. In the baffle window, these two types of streams tend to mix dynamically, and behind the baffle window, the direction of movement is additionally altered. As a consequence, extensive vortex patterns develop at the bottom of the shell. Due to the proportionality in the variations of the velocity of the central stream and bypass streams for the flow parameters investigated in the paper, we can conclude that the presence of vortex patterns in the baffle window is not dependent on the inflow rate Q. Therefore, we should forecast that the factor responsible for the intensity and characteristics the vortex zone in the baffle window is associated with the geometric parameters. The streamlines analysis indicates considerable conformity of the CFD and PIV results. Only the area between the shell and the first row of tubes is characterized by significant differences in the streamlines. These results are also reflected in the distribution of the vertical velocity profiles (lines 5–8 in Figures 14–16). In order to obtain knowledge about the dynamics of large vortex

cells in the lower part of the shell side, the variability of the velocity of liquid flow in this area was examined in the further part of the study.

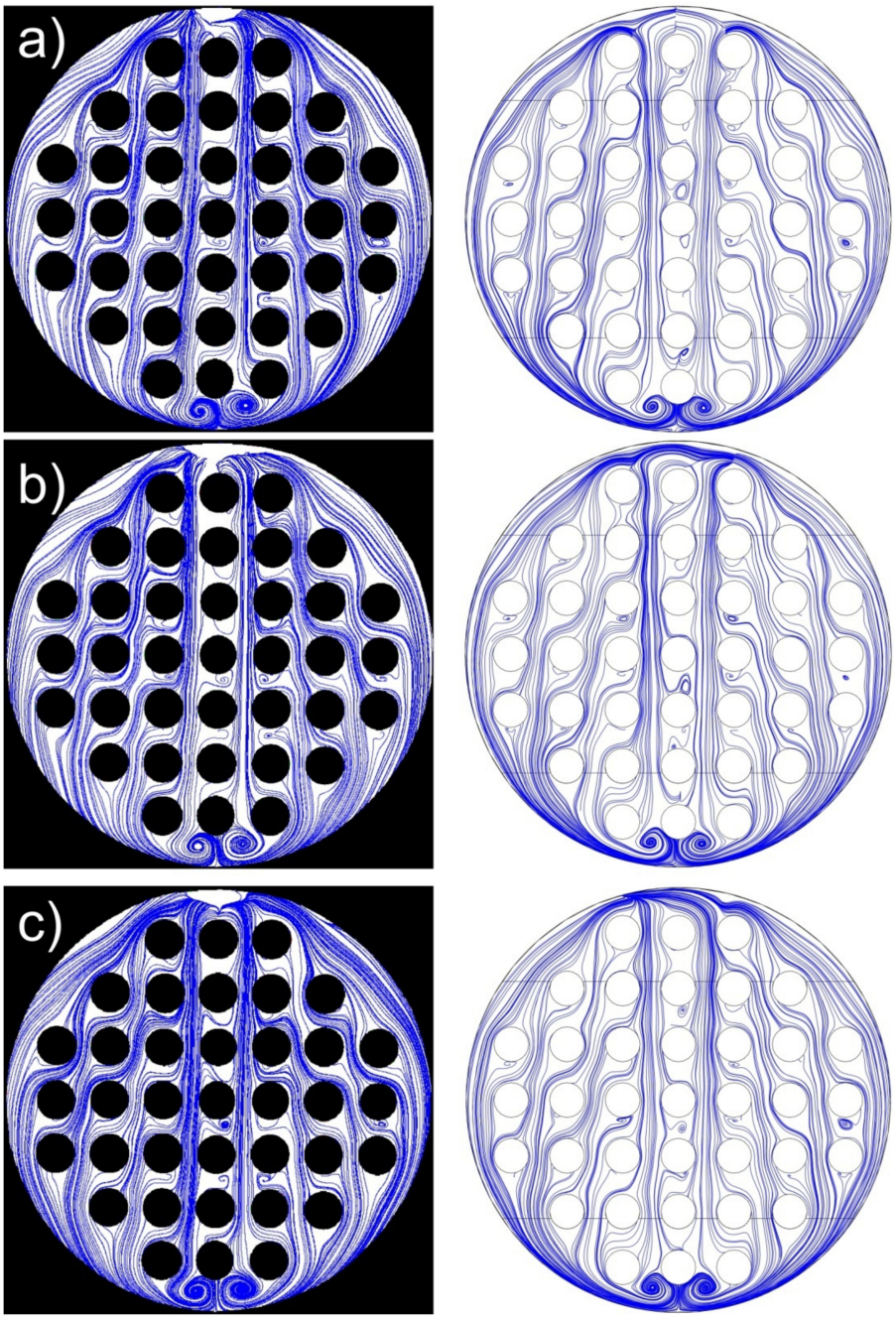

Figure 18. Comparison of streamlines PIV (left row) and CFD (right row) for various liquid flow rate: (**a**) Q = 5 m^3/h, (**b**) Q = 7.5 m^3/h, and (**c**) Q = 10 m^3/h.

The occurrence of displacement of vortex patterns is also noteworthy. This is illustrated in Figure 19 by determining the variations in the velocity in time at point F, located in the middle of the distance between the final tube in the middle row and on the shell wall of the heat exchanger. Taking into account the theoretical velocity distribution in the vortex structure, characterized by an increase in velocity on the borders of the vortex and a decrease in velocity in its core, it can be demonstrated that in the area of the border rows of the tubes, we have to do with recurrent fluctuations in the vortex location. Regardless of the flow rate Q, these fluctuations are at a similar level (see dynamic velocity V/v_{in}

changes in Figure 19). Thus, it is possible that the observed mechanism of the vortex displacement may generate erosive interactions on the outer surfaces of tubes in such regions, occurring by analogy to the erosive interactions inside the tubes, in tube bends [44]. An additional factor that supports such observation is associated with the fact that contaminants accumulate on the bottom of the STHE shell, which may enhance the erosive effect of the vortex structures. This area should therefore be monitored for accelerated erosive wear. In extreme conditions, the fluctuation of vortices in the lower part of the shell side could interfere in the symmetry of the flow and contribute to imbalanced heat transfer. The solution that could counteract this situation could be associated with geometrical modifications in the form of bars preventing the displacement of vortices.

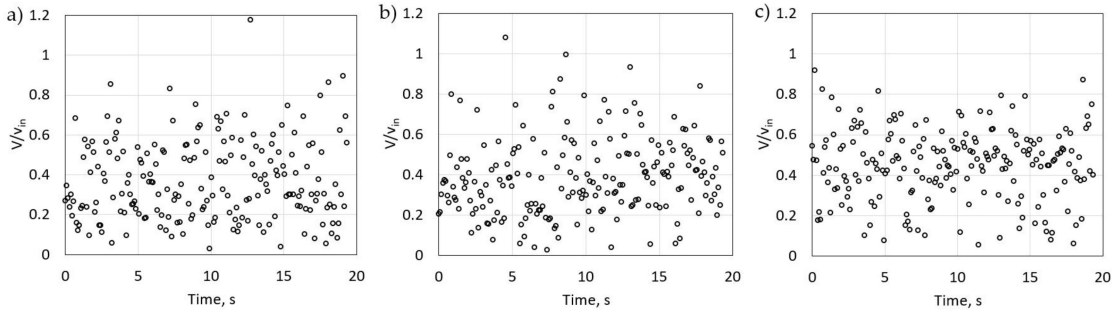

Figure 19. Variations in velocity for point F in time for (**a**) Q = 5 m^3/h, (**b**) Q = 7.5 m^3/h, and (**c**) Q = 10 m^3/h.

4. Conclusions

On the basis of the numerical and experimental investigations of the shell side in STHEs, it was found that the information in the images of the liquid velocity fields is sufficient for the purposes of the effective evaluation of flow maldistribution. On the basis of the analysis, the following conclusions were formulated:

1. The study presented a method of eliminating perspective phenomenon on the recorded image of the shell side resulting from the geometric modification involving the removal of a section of the tube bundle behind the last baffle. This procedure extends the area of the image feasible for the planar PIV analysis of the full cross-section resulting from the actual geometry of the shell side. At the same time, the variations in the hydrodynamic parameters resulting from the removal of a section of the tube bundle remain at an acceptable level. The maximum differences of the dimensionless parameters defining the velocities differ by a maximum of 3.5%, also pressure drops vary within a small range that does not exceed 3%.
2. The results obtained in the validation process (in relation to the values of pressure drops obtained on the basis of experimental tests and the values of average and maximum velocities - in relation to the PIV tests) of the adopted numerical strategy allow us to conclude that, in case of the numerical calculations in the shell side of a STHE, the use of hybrid mesh with tetrahedral cells and the standard k-ε model with RANS enables reliable analysis of the flow inside the heat exchanger.
3. Liquid flow maldistributions were identified in the studies. Two central streams could be distinguished, flowing in parallel on both sides of the middle row of tubes. Between the tubes in the middle row, regardless of the flow rate Q, there were cyclic areas with reduced velocity and high vortex generation potential. Their occurrence was considered unfavorable due to their negative role in forming heat transfer parameters.
4. In the areas on the outer sides of the central streams there were symmetrical oblique streams, where the regions of reduced velocities did not extend to the subsequent tube rows. Oblique liquid flow in an in-line layout transforms the flow patterns toward structures specific to liquid flow into a staggered layout.

5. An increase in the velocity gradient was observed with an increase in the flow rate Q for the successive tube rows. The highest velocity gradient was noted for line 1 and the lowest for line 4 located in Figure 13. On this basis, it was concluded that the evolution of velocity in the tested geometry is an important factor that should be taken into account in thermal calculations.
6. The phenomenon of the displacement of vortices in the baffle window was observed. This can potentially lead to unfavorable erosive effects on tubes within the vortex zone. Structural elements in the form of bars in the lower part of the exchanger shell may prevent the displacement of vortices in the baffle window. Such modifications are likely to extend the effective service life of the heat exchanger.

Author Contributions: Conceptualization, G.L.; methodology, M.W. and S.K.; software, M.W. and G.L.; validation, D.Z., M.W. and S.K.; formal analysis, M.W. and G.L.; investigation, G.L. and M.W.; resources, S.K.; data curation, S.K.; writing—Original draft preparation, G.L. and M.W.; writing—Review and editing, D.Z.; visualization, G.L. and M.W.; supervision, G.L.; project administration, S.K. and D.Z.; funding acquisition, D.Z. All authors have read and agreed to the published version of the manuscript.

Funding: This research was carried out with the support of the Interdisciplinary Centre for Mathematical and Computational Modelling (ICM) University of Warsaw under grant no G73-10.

Conflicts of Interest: The authors declare no conflict of interest

References

1. Bhutta, M.M.A.; Hayat, N.; Bashir, M.H.; Khan, A.R.; Ahmad, K.N.; Khan, S. CFD applications in various heat exchangers design: A review. *Appl. Therm. Eng.* **2012**, *32*, 1–12. [CrossRef]
2. Zhang, Z.; Li, Y. CFD simulation on inlet configuration of plate-fin heat exchangers. *Cryogenics* **2003**, *43*, 673–678. [CrossRef]
3. Yataghene, M.; Pruvost, J.; Fayolle, F.; Legrand, J. CFD analysis of the flow pattern and local shear rate in a scraped surface heat exchanger. *Chem. Eng. Process. Process. Intensif.* **2008**, *47*, 1550–1561. [CrossRef]
4. Zhang, L.-Z. Flow maldistribution and thermal performance deterioration in a cross-flow air to air heat exchanger with plate-fin cores. *Int. J. Heat Mass Transf.* **2009**, *52*, 4500–4509. [CrossRef]
5. Kim, M.I.; Lee, Y.; Kim, B.W.; Lee, D.H.; Song, W.S. CFD modeling of shell-and-tube heat exchanger header for uniform distribution among tubes. *Korean J. Chem. Eng.* **2009**, *26*, 359–363. [CrossRef]
6. Ozden, E.; Tari, I. Shell side CFD analysis of a small shell-and-tube heat exchanger. *Energy Convers. Manag.* **2010**, *51*, 1004–1014. [CrossRef]
7. Wang, Q.Y.; Dong, M.L. Characteristics of fluid flow and heat transfer in shell side of heat exchangers with longitudinal flow of shell side fluid with different supporting structures. In Proceedings of the International Conference on Power Engineering, Singapore, 3–6 December 2007.
8. Wang, Q.; Chen, Q.; Chen, G.; Zeng, M. Numerical investigation on combined multiple shell-pass shell-and-tube heat exchanger with continuous helical baffles. *Int. J. Heat Mass Transf.* **2009**, *52*, 1214–1222. [CrossRef]
9. Mohammadi, K.; Heidemann, W.; Muller-Steinhagen, H. Numerical investigation of the effect of baffle orientation on heat transfer and pressure drop in a shell and tube heat exchanger with leakage flows. *Heat Transf. Eng.* **2009**, *30*, 1123–1135. [CrossRef]
10. Raj, V.A.A.; Velraj, R. Heat transfer and pressure drop studies on a PCM-heat exchanger module for free cooling applications. *Int. J. Therm. Sci.* **2011**, *50*, 1573–1582. [CrossRef]
11. Sun, Y.; Wang, X.; Long, R.; Yuan, F.; Yang, K. Numerical investigation and optimization on shell side performance of a shell and tube heat exchanger with inclined trefoil-hole baffles. *Energies* **2019**, *12*, 4138. [CrossRef]
12. Jun, S.; Puri, V.M. 3D milk-fouling model of plate heat exchangers using computational fluid dynamics. *Int. J. Dairy Technol.* **2005**, *58*, 214–224. [CrossRef]
13. de Bonis, M.V.; Ruocco, G. Conjugate fluid flow and kinetics modeling for heat exchanger fouling simulation. *Int. J. Therm. Sci.* **2009**, *48*, 2006–2012. [CrossRef]
14. Iwaki, C.; Cheong, K.-H.; Monji, H.; Matsui, G. PIV measurement of the vertical cross-flow structure over tube bundles. *Exp. Fluids* **2004**, *37*, 350–363. [CrossRef]

15. Iwaki, C.; Cheong, K.-H.; Monji, H.; Matsui, G. Vertical, bubbly, cross-flow characteristics over tube bundles. *Exp. Fluids* **2005**, *39*, 1024–1039. [CrossRef]
16. Zhang, X.; Daghrah, M.; Wang, Z.; Liu, Q.; Jarman, P.; Negro, M. Experimental verification of dimensional analysis results on flow distribution and pressure drop for disc-type windings in OD cooling modes. *IEEE Trans. Power Deliv.* **2017**, *33*, 1647–1656. [CrossRef]
17. Talapatra, S.; Farrell, K. Planar PIV experiments inside a transparent shell-and-tube exchanger. *SME Int. Mech. Eng. Congr. Expo. Proc.* **2014**, *7*. [CrossRef]
18. Bouhairie, S.; Talapatra, S.; Farrell, K. Turbulent flow in a no-tube-in-window shell-and-tube heat exchanger: CFD vs PIV. *ASME Int. Mech. Eng. Congr. Expo. Proc.* **2014**, *7*. [CrossRef]
19. Talapatra, S.; Farrell, K. Two-phase flow regimes in exchangers and piping: Part 1. *ASME Int. Mech. Eng. Congr. Expo. Proc* **2015**, *57465*. [CrossRef]
20. Wang, K.; Zhang, Z.; Liu, Q.; Tu, X.; Kim, H.-B. PIV measurement of tube-side in a shell and tube heat exchanger. *Pol. J. Chem. Technol.* **2018**, *20*, 60–66. [CrossRef]
21. Liu, P.; Zheng, N.; Rui, L.; Shan, F.; Liu, Z.; Liu, W. PIV measurement of flow structures in a circular heat exchange tube with central slant rod inserts. *Energy Procedia* **2017**, *142*, 3793–3798. [CrossRef]
22. Lee, S.; Delgado, M.; Hassan, Y.; Lee, S.J. Experimental investigation of the isothermal flow field across slant 5-tube bundles in helically coiled steam generator geometry using PIV. *Nucl. Eng. Des.* **2018**, *338*, 261–268. [CrossRef]
23. Delgado, M.; Lee, S.; Hassan, Y.; Anand, N.K. Flow visualization study at the interface of alternating pitch tube bundles in a model helical coil steam generator using particle image velocimetry. *Int. J. Heat Mass Transf.* **2018**, *122*, 614–628. [CrossRef]
24. Delgado, M.; Hassan, Y.; Anand, N.K. Experimental flow visualization study using particle image velocimetry in a helical coil steam generator with changing lateral pitch geometry. *Int. J. Heat Mass Transf.* **2019**, *133*, 756–768. [CrossRef]
25. Im, S.; Kim, H.T.; Rhee, B.W.; Sung, H.J. PIV measurements of the flow patterns in a CANDU-6 model. *Ann. Nucl. Energy* **2016**, *98*, 1–11. [CrossRef]
26. Chang, T.-H.; Lee, C.-H.; Lee, H.-S.; Lee, K.-S. Velocity profiles between two baffles in a shell and tube heat exchanger. *J. Therm. Sci.* **2015**, *24*, 356–363. [CrossRef]
27. Wen, J.; Yang, H.; Wang, S.; Gu, X. PIV experimental investigation on shell-side flow patterns of shell and tube heat exchanger with different helical baffles. *Int. J. Heat Mass Transf.* **2017**, *104*, 247–259. [CrossRef]
28. Fluent Inc. In *FLUENT 6.3 User s Guide. Options*; Fluent Inc. Centerra Resource Park 10 Cavendish Court: Lebanon, NH, USA, 2006.
29. Yang, J.; Liu, W. Numerical investigation on a novel shell-and-tube heat exchanger with plate baffles and experimental validation. *Energy Convers. Manag.* **2015**, *101*, 689–696. [CrossRef]
30. Shahril, S.; Quadir, G.; Amin, N.; Badruddin, I.A. Thermo hydraulic performance analysis of a shell-and-double concentric tube heat exchanger using CFD. *Int. J. Heat Mass Transf.* **2017**, *105*, 781–798. [CrossRef]
31. el Maakoul, A.; Laknizi, A.; Saadeddine, S.; el Metoui, M.; Zaite, A.; Meziane, M.; Ben-Abdellah, A. Numerical comparison of shell-side performance for shell and tube heat exchangers with trefoil-hole, helical and segmental baffles. *Appl. Therm. Eng.* **2016**, *109*, 175–185. [CrossRef]
32. Pal, E.; Kumar, I.; Joshi, J.; Maheshwari, N. CFD simulations of shell-side flow in a shell-and-tube type heat exchanger with and without baffles. *Chem. Eng. Sci.* **2016**, *143*, 314–340. [CrossRef]
33. You, Y.; Chen, Y.; Xie, M.; Luo, X.; Jiao, L.; Huang, S. Numerical simulation and performance improvement for a small size shell-and-tube heat exchanger with trefoil-hole baffles. *Appl. Therm. Eng.* **2015**, *89*, 220–228. [CrossRef]
34. Leoni, G.B.; Klein, T.S.; Medronho, R.D.A. Assessment with computational fluid dynamics of the effects of baffle clearances on the shell side flow in a shell and tube heat exchanger. *Appl. Therm. Eng.* **2017**, *112*, 497–506. [CrossRef]
35. Nogueira, X.; Taylor, B.J.; Gomez, H.; Colominas, I.; Mackley, M.R. Experimental and computational modeling of oscillatory flow within a baffled tube containing periodic-tri-orifice baffle geometries. *Comput. Chem. Eng.* **2013**, *49*, 1–17. [CrossRef]

36. Ambekar, A.S.; Sivakumar, R.; Anantharaman, N.; Vivekenandan, M. CFD simulation study of shell and tube heat exchangers with different baffle segment configurations. *Appl. Therm. Eng.* **2016**, *108*, 999–1007. [CrossRef]
37. Versteeg, H.K.; Malalasekera, W.; Orsi, G.; Ferziger, J.H.; Date, A.W.; Anderson, J.D. *An Introduction to Computational Fluid Dynamics—The Finite Volume Method*; Pearson Education Limited: London, UK, 1995; ISBN 9783540594345.
38. Adrian, R.J.; Westerweel, J. *Particle Image Velocimetry*; Cambridge University Press: New York, NY, USA, 2011; ISBN 978-0-521-44008-0.
39. Tropea, C.; Yarin, A.L.; Foss, J.F. *Springer Handbook of Experimental Fluid Mechanics*; Springer: Berlin/Heidelberg, Germany, 2007.
40. Binyet, E.M.; Chang, J.-Y.; Huang, C.-Y. Flexible plate in the wake of a square cylinder for piezoelectric energy harvesting—Parametric study using fluid–structure interaction modeling. *Energies* **2020**, *13*, 2645. [CrossRef]
41. Matsubara, T.; Shima, Y.; Aono, H.; Ishikawa, H.; Segawa, T. Effects of jet induced by string-type plasma actuator on flow around three-dimensional bluff body and drag force. *Energies* **2020**, *13*, 872. [CrossRef]
42. Liu, D.; Wang, Y.Z.; Shi, W.; Kim, H.-B.; Tang, A. Slit wall and heat transfer effect on the taylor vortex Flow. *Energies* **2015**, *8*, 1958–1974. [CrossRef]
43. Paul, S.; Tachie, M.F.; Ormiston, S. Experimental study of turbulent cross-flow in a staggered tube bundle using particle image velocimetry. *Int. J. Heat Fluid Flow* **2007**, *28*, 441–453. [CrossRef]
44. Gogolin, A.; Wasilewski, M.; Ligus, G.; Wojciechowski, S.; Gapiński, B.; Krolczyk, J.B.; Zajac, D.; Krolczyk, G. Influence of geometry and surface morphology of the U-tube on the fluid flow in the range of various velocities. *Measurement* **2020**, *164*, 108094. [CrossRef]